Available online at www.sciencedirect.com
ScienceDirect
J. Vis. Commun. Image R. 18 (2007) 322–330
JOURNAL OF VISUAL Communication & IMAGE Representation
www.elsevier.com/locate/jvci

Image restoration combining a total variational filter and a fourth-order filter

Fang Li [a,*], Chaomin Shen [b], Jingsong Fan [a], Chunli Shen [a]

[a] Department of Mathematics, East China Normal University, Shanghai 200062, China
[b] Joint Laboratory for Imaging Science & Technology, and Department of Computer Science, East China Normal University, Shanghai 200062, China

Received 4 March 2006; accepted 10 April 2007
Available online 3 May 2007

Abstract

In this paper, a noise removal algorithm based on variational method and partial differential equations (PDEs) is proposed. It combines a total variational filter (ROF filter) with a fourth-order PDE filter (LLT filter). The combined algorithm takes the advantage of both filters since it is able to preserve edges while avoiding the staircase effect in smooth regions. The existence and uniqueness of a solution to the minimization problem is established. Experimental results illustrate the effectiveness of the model in image restoration.

Keywords: Image restoration; Total variation; Fourth-order filter; BV space; BV^2 space

1. Introduction

In this paper, we study the problem of image restoration. The essential idea for image restoration is to filter out noise while preserving important features such as edges.

In general, an image can be decomposed into two kinds of areas: smooth regions (regions with a smooth change in the intensity value), and discontinuities (for example, jumps such as edges of an object). The discontinuities are usually the features of interest. Therefore, if an image is viewed as a function with discontinuities, we should study this function in a suitable function space. The Sobolev space fails in this case. The space of functions with bounded variation, called BV space, is suitable to describe functions with discontinuities [1]. Here, we recall the definition of BV space.

Definition 1.1. Let $\Omega \subset R^n$ be an open subset with Lipschitz boundary. Define $BV(\Omega)$ (BV space) as the subspace of functions $u \in L^1(\Omega)$ such that the following quantity, called the BV semi-norm, is finite:

$$\int_\Omega |Du| := \sup\left\{\int_\Omega u \operatorname{div}(\varphi)\mathrm{d}x | \varphi \in C_c^1(\Omega, R^n), |\varphi| \leqslant 1\right\}.$$

With the norm $\|u\|_{BV(\Omega)} = \int_\Omega |Du| + \|u\|_{L^1(\Omega)}$, $BV(\Omega)$ is a Banach space [1,2].

Many variational methods in image processing involve BV space [3–6]. For our purpose, the most related one is the total variation minimization proposed by Rudin, Osher and Fatemi [6] (the ROF model):

$$\min_{u\in BV(\Omega)\cap L^2(\Omega)} \left\{E(u) = \int_\Omega |Du| + \frac{\lambda}{2}\int_\Omega (f-u)^2 \mathrm{d}x\right\}. \tag{1.1}$$

The corresponding partial differential equation (PDE) of (1.1) is a second-order equation. The ROF model does an excellent job in preserving edges since the diffusion with this PDE is along edges. The ROF model, together with its improved version, the weighted ROF model, has been extensively studied and proven to be efficient for preserving edges [3,4,7,8].

However, the ROF model often causes 'staircase' effects [4,9,10] since it favors solutions that are piecewise constant.

* Corresponding author.
E-mail address: lifangswnu@126.com (F. Li).

1047-3203/$ - see front matter
doi:10.1016/j.jvcir.2007.04.005

Here, staircase means that smooth regions with noise are processed into piecewise constant regions after using the ROF model. Staircase solutions fail to satisfy the eye and they can develop 'false edges' that do not exist in the true image.

In the recent decade, high-order PDEs (typically, fourth-order PDEs) have been introduced in image restoration [11–19]. The theoretical analysis in [20,21] shows that fourth-order equations have advantages over second-order equations in some aspects. First of all, fourth-order linear or nonlinear diffusion damps oscillations much faster than second-order diffusion. Furthermore, fourth-order PDEs usually evolve an observed image toward an 'almost smooth' image. This is believed to be a better approximation to a natural image than a piecewise constant approximation in smooth regions [13]. Therefore, the staircase effect will be reduced and the image will look more natural. This has been verified numerically [13,14,17]. Thus, we can reasonably conclude that fourth-order diffusion performs better than the ROF model in the aspect of recovery of smooth regions.

An example of a fourth-order equation is the model proposed by Lysaker, Lundervold and Tai (the LLT model). They propose a second-order functional:

$$\min_{u\in W^{2,1}(\Omega)\cap L^2(\Omega)}\left\{E(u)=\int_\Omega|\nabla^2 u|\mathrm{d}x+\frac{\lambda}{2}\int_\Omega(f-u)^2\mathrm{d}x\right\}, \tag{1.2}$$

where $|\nabla^2 u|:=\sqrt{u_{xx}^2+u_{xy}^2+u_{yx}^2+u_{yy}^2}$. The corresponding diffusion equation of (1.2) is a fourth-order filter.

It is natural to investigate a model combining the advantages of the ROF model and the LLT model. Lysaker and Tai [22] proposed an iterative restoration method making use of a weighting function to combine the results of model (1.1) and (1.2). However, the construction of the weighting function is not quite intuitive. In this paper, we aim to construct an energy functional that combines (1.1) and (1.2) more naturally and efficiently.

Similar to the case where the Sobolev space $W^{1,1}(\Omega)$ is replaced by $\mathrm{BV}(\Omega)$, the Sobolev space $W^{2,1}(\Omega)$ can be replaced by a new space called BV^2 space which is composed of functions with bounded variation in the second-order derivatives [16,17]. The definition of BV^2 space is given as follows.

Definition 1.2. Let $\Omega\subset R^n$ be an open subset with Lipschitz boundary. Define $\mathrm{BV}^2(\Omega)$ as the subspace of functions $u\in L^1(\Omega)$ such that the following quantity, called the BV^2 semi-norm, is finite:

$$\int_\Omega|D^2u|:=\sup\left\{\int_\Omega\sum_{i,j=1}^n u\partial_j\partial_i\varphi^{ij}\mathrm{d}x|\varphi\in C_c^2(\Omega,R^{n\times n}),|\varphi|\leqslant 1\right\},$$

where $|\varphi(x)|=\sqrt{\sum_{i=1}^n\sum_{j=1}^n(\varphi^{ij})^2}$.

Similar to weighted BV space, we introduce weighted BV^2 space denoted by $g-\mathrm{BV}^2(\Omega)$. A function u belongs to $g-\mathrm{BV}^2(\Omega)$ if $u\in L^1(\Omega)$ and satisfies

$$\int_\Omega g|D^2u|:=\sup\left\{\int_\Omega\sum_{i,j=1}^n u\partial_j\partial_i\varphi^{ij}\mathrm{d}x|\varphi\in C_c^2(\Omega,R^{n\times n}),|\varphi|\leqslant g\right\}<\infty,$$

where g is a nonnegative function.

Using the similar technique done in BV space ([1], Theorem 1 in Section 5.1, Theorems 1 and 4 in Section 5.2), we can establish the structure theorem, the lower semi-continuity and the compactness theorem in BV^2 space. Moreover, we can also prove the lower semi-continuity and the compactness theorem in weighted BV^2 space with methods similar to what Chen [6] used in weighted BV space.

Note that our definition of $\mathrm{BV}^2(\Omega)$ is a little different from that in [16,17]. $\mathrm{BV}^2(\Omega)$ is defined as a subspace of functions $u\in L^2(\Omega)$ in [16,17] while we, on the other hand, use $u\in L^1(\Omega)$. In this way, we can give a natural definition of the BV^2 norm, that is, $\|u\|_{\mathrm{BV}^2(\Omega)}=\int_\Omega|D^2u|+\|u\|_{L^1(\Omega)}$. By the lower semi-continuity and the compactness theorem in BV^2 space, we can deduce that $\mathrm{BV}^2(\Omega)$ is a Banach space with this norm. Similar result is true in weighted BV^2 space.

Also note that $\int_\Omega|D^2u|=\int_\Omega|\nabla^2u|\,\mathrm{d}x$ when $u\in W^{2,1}(\Omega)$. In fact, by the divergence theorem,

$$\begin{aligned}\sup_{|\varphi|\leqslant1}\int_\Omega\sum_{i,j=1}^n u\partial_j\partial_i\varphi^{ij}\mathrm{d}x&=\sup_{|\varphi|\leqslant1}\int_\Omega-\sum_{i,j=1}^n\partial_j u\partial_i\varphi^{ij}\mathrm{d}x\\&=\sup_{|\varphi|\leqslant1}\int_\Omega\sum_{i,j=1}^n\partial_i\partial_j u\varphi^{ij}\mathrm{d}x.\end{aligned}$$

The supremum in the last equality can be attained by $\varphi^{ij}=\eta\frac{\partial_i\partial_j u}{|\nabla^2u|}$, where $|\nabla^2u|=\sqrt{u_{xx}^2+u_{xy}^2+u_{yx}^2+u_{yy}^2}$, and η is the cut off function that is 0 near the boundary, 1 in the subset $\Omega'\subset\subset\Omega$ and varies smoothly between these two values. Then

$$\int_\Omega|D^2u|=\int_\Omega|\nabla^2u|\mathrm{d}x.$$

The remainder of the paper is organized as follows: in Section 2, we propose our model for image restoration in the space $\mathrm{BV}(\Omega)\cap\mathrm{BV}^2(\Omega)\cap L^2(\Omega)$ and prove the existence and uniqueness of a solution to our minimization problem. In Section 3, for the convenience of numerical computation, we derive the associated heat flow for our minimization problem in the subspace $W^{1,1}(\Omega)\cap W^{2,1}(\Omega)\cap L^2(\Omega)$ using the steepest descent method. In Section 4, we give the numerical scheme in detail. Meanwhile, we employ experimental results and parameter estimates to demonstrate the effectiveness of our algorithm. Finally, we conclude our paper in Section 5.

2. The proposed model and minimization problem

Let u: $\Omega\subset R^2\to R$ be a gray scale image. Based on weighted BV space and weighted BV^2 space, our model is proposed as follows:

$$\min_{u\in \mathrm{BV}(\Omega)\cap \mathrm{BV}^2(\Omega)\cap L^2(\Omega)} \int_\Omega (1-g)|Du| + \int_\Omega g|D^2u|\mathrm{d}x + \frac{\lambda}{2}\int_\Omega (u-u_0)^2\mathrm{d}x, \tag{2.1}$$

where $g(x)$ is a stopping function chosen as $g=\frac{1}{1+\gamma+k|\nabla G_\sigma * 0|^2}$; $\lambda>0$ is the coefficient of the fidelity term; $\gamma>0$ is a very small positive number added to ensure $g<1$ that is needed in theoretical analysis; $k>0$ is the contrast factor; G_σ is the Gaussian kernel and σ denotes the standard deviation.

Eq. (2.1) is a natural combination of the ROF model and the LLT model in the space $u\in \mathrm{BV}(\Omega)\cap \mathrm{BV}^2(\Omega)\cap L^2(\Omega)$. By the selection of g, the ROF minimization plays the main role when $|G_\sigma * \nabla u_0|$ is large (large $|G_\sigma * \nabla u_0|$ correspond to the locations where edges most likely appear); the LLT minimization plays the main role when $|G_\sigma * \nabla u_0|$ is small (small $|G_\sigma * \nabla u_0|$ correspond to the locations with smooth signals). Thus, our model has the advantage of preserving edges, inherited from the ROF model, and the advantage of better restoration (less staircase effects) in smooth regions, inherited from the LLT model.

Theorem 2.1. *Assume $u_0\in BV(\Omega)\cap BV^2(\Omega)\cap L^\infty(\Omega)$, then the energy (2.1) has a unique minimizer $u_*\in BV(\Omega)\cap BV^2(\Omega)\cap L^\infty(\Omega)$.*

Proof. For an arbitrary $\varepsilon>0$, consider the following minimization problem

$$\min_{u\in W^{1,1+\varepsilon}(\Omega)\cap W^{2,1+\varepsilon}(\Omega)\cap L^2(\Omega)} \left\{\int_\Omega \frac{1-g}{1+\varepsilon}|\nabla u|^{1+\varepsilon} + \int_\Omega \frac{g}{1+\varepsilon}|\nabla^2 u|^{1+\varepsilon}\mathrm{d}x + \frac{\lambda}{2}\int_\Omega (u-u_0)^2\mathrm{d}x\right\}. \tag{2.2}$$

Clearly, $\frac{1}{1+\gamma+C\|u_0\|_\infty^2}\leqslant g\leqslant \frac{1}{1+\gamma}$ from the properties of Gaussian kernel. Then the weighted function g and $1-g$ are both positively bounded from below. Therefore the functional (2.2) is strictly convex, coercive and weak lower semi-continuous in a reflexive Banach space $W^{1,1+\varepsilon}(\Omega)\cap W^{2,1+\varepsilon}(\Omega)\cap L^2(\Omega)$. Therefore (2.2) has a unique solution $u_\varepsilon\in W^{1,1+\varepsilon}(\Omega)\cap W^{2,1+\varepsilon}(\Omega)\cap L^2(\Omega)$ by the standard argument.

Fix ε, $t\geqslant 0$, and let $v=\min\{u_\varepsilon, t\}$. Then $v\in W^{1,1+\varepsilon}(\Omega)\cap W^{2,1+\varepsilon}(\Omega)\cap L^2(\Omega)$ with

$$\nabla v=\begin{cases}\nabla u_\varepsilon & \text{if } u_\varepsilon<t\\ 0, & \text{if } u_\varepsilon\geqslant t\end{cases} \quad\text{and}\quad |\nabla^2 v|=\begin{cases}|\nabla^2 u_\varepsilon|, & \text{if } u_\varepsilon<t\\ 0, & \text{if } u_\varepsilon\geqslant t\end{cases}$$

Since u_ε is a minimizer, we have

$$\int_\Omega \frac{1-g}{1+\varepsilon}|\nabla u_\varepsilon|^{1+\varepsilon} + \int_\Omega \frac{g}{1+\varepsilon}|\nabla^2 u_\varepsilon|^{1+\varepsilon}\mathrm{d}x + \frac{\lambda}{2}\int_\Omega (u_\varepsilon-u_0)^2\mathrm{d}x \leqslant \int_\Omega \frac{1-g}{1+\varepsilon}|\nabla v|^{1+\varepsilon} + \int_\Omega \frac{g}{1+\varepsilon}|\nabla^2 v|^{1+\varepsilon}\mathrm{d}x + \frac{\lambda}{2}\int_\Omega (v-u_0)^2\mathrm{d}x. \tag{2.3}$$

By direct calculation, we obtain

$$\int_{\{u_\varepsilon\geqslant t\}} \frac{1-g}{1+\varepsilon}|\nabla u_\varepsilon|^{1+\varepsilon} + \int_{\{u_\varepsilon\geqslant t\}} \frac{g}{1+\varepsilon}|\nabla^2 u_\varepsilon|^{1+\varepsilon}\mathrm{d}x + \frac{\lambda}{2}\int_{\{u_\varepsilon\geqslant t\}} (u_\varepsilon-u_0)^2\mathrm{d}x \leqslant \frac{\lambda}{2}\int_{\{u_\varepsilon\geqslant t\}} (v-u_0)^2\mathrm{d}x.$$

Hence

$$\int_{\{u_\varepsilon\geqslant t\}} (u_\varepsilon-u_0)^2\mathrm{d}x \leqslant \int_{\{u_\varepsilon\geqslant t\}} (t-u_0)^2\mathrm{d}x. \tag{2.4}$$

By setting $t=\|u_0\|_{L^\infty(\Omega)}$, if ess sup $u_\varepsilon>t$, then

$$\int_{\{u_\varepsilon\geqslant t\}} (u_\varepsilon-u_0)^2\mathrm{d}x > \int_{\{u_\varepsilon\geqslant t\}} (t-u_0)^2\mathrm{d}x,$$

which contradicts (2.4). Hence ess sup $u_\varepsilon\leqslant |u_0|_{L^\infty(\Omega)}$.

Applying a similar argument to $v=\max\{u_\varepsilon, -t\}$ for $t=\|u_0\|_{L^\infty(\Omega)}$, we get ess inf $u_\varepsilon\geqslant -|u_0|_{L^\infty(\Omega)}$ and hence $\|u_\varepsilon\|_{L^\infty(\Omega)}\leqslant \|u_0\|_{L^\infty(\Omega)}$. Taking $v=0$ in (2.9), then $\{u_\varepsilon\}$ is bounded in $W^{1,1+\varepsilon}\cap W^{2,1+\varepsilon}(\Omega)\cap L^2(\Omega)\subset \mathrm{BV}(\Omega)\cap \mathrm{BV}^2(\Omega)\cap L^2(\Omega)$. Thus there is a $u_*\in \mathrm{BV}(\Omega)\cap \mathrm{BV}^2(\Omega)\cap L^2(\Omega)$ and a subsequence, also denoted by $\{u_\varepsilon\}$, such that $u_\varepsilon\to u_*$ strongly in $L^1(\Omega)$, weakly in $L^2(\Omega)$ and $u_\varepsilon\to u_*$ a.e. in Ω as $\varepsilon\to 0$. Letting $\varepsilon\to 0$ and using (2.2), we get from (2.3) that

$$\int_\Omega (1-g)|Du_*| + \frac{1}{2}\int_\Omega g|D^2u_*|\mathrm{d}x + \frac{\lambda}{2}\int_\Omega (u_*-u_0)^2\mathrm{d}x \leqslant \int_\Omega (1-g)|Dv| + \frac{1}{2}\int_\Omega g|D^2v|\mathrm{d}x + \frac{\lambda}{2}\int_\Omega (v-u_0)^2\mathrm{d}x$$

for all $v\in W^{1,1+\varepsilon}\cap W^{2,1+\varepsilon}(\Omega)\cap L^2(\Omega)$. Since for all $v\in \mathrm{BV}(\Omega)\cap \mathrm{BV}^2(\Omega)\cap L^2(\Omega)$,$v$ can be approximated by a sequence $v_n\in C^\infty(\bar\Omega)$ satisfying $\int_\Omega(1-g)|Dv_n|\to\int_\Omega(1-g)|Dv|$, $\int_\Omega g|D^2v_n|\to\int_\Omega g|D^2v|$, and $v_n\to v$ strongly in $L^1(\Omega)$ and $L^2(\Omega)$ from the construction of v_n [11]. Therefore, the above inequality holds for all $v\in \mathrm{BV}(\Omega)\cap \mathrm{BV}^2(\Omega)\cap L^2(\Omega)$. Hence u_* is a minimizer to the energy functional (2.1). By the uniform L^∞ bound for u_ε and the convergence of u_ε to u_* a.e. in Ω, we have $u_*\in L^\infty(\Omega)$ with $\|u_*\|_{L^\infty(\Omega)}\leqslant \|u_0\|_{L^\infty(\Omega)}$. Thus we have proven the existence of a minimizer $u_*\in L^\infty(\Omega)$.

Uniqueness follows from the strict convexity of the energy functional in (2.1). □

3. Flow associated to the energy functional

Numerically, we use the following minimization problem to approximate (2.1):

$$\min_{u\in W^{1,1}(\Omega)\cap W^{2,1}(\Omega)\cap L^2(\Omega)} \int_\Omega (1-g)|\nabla u| + \int_\Omega g|\nabla^2 u|\mathrm{d}x + \frac{\lambda}{2}\int_\Omega (u-u_0)^2\mathrm{d}x. \tag{3.1}$$

Next, we will derive the evolution equation of energy (3.1).

For simplicity, we introduce the notation $|\nabla^2 u| = \sqrt{u_{xx}^2 + u_{xy}^2 + u_{yx}^2 + u_{yy}^2} = \sqrt{\nabla u_x \cdot \nabla u_x + \nabla u_y \cdot \nabla u_y}$. Then the directional (Gateaux) derivative of E at u in the direction of v is given by

$$\begin{aligned}
&\frac{\mathrm{d}}{\mathrm{d}\varepsilon}|_{\varepsilon=0} E(u+\varepsilon v)\\
&= \frac{\mathrm{d}}{\mathrm{d}\varepsilon}|_{\varepsilon=0}\left\{\int_\Omega (1-g)|\nabla u + \varepsilon\nabla v|\mathrm{d}x\mathrm{d}y\right.\\
&\quad + \int_\Omega g\sqrt{(\nabla u_x + \varepsilon\nabla v_x)\cdot(\nabla u_x + \varepsilon\nabla v_x) + (\nabla u_y + \varepsilon\nabla v_y)\cdot(\nabla u_y + \varepsilon\nabla v_y)}\mathrm{d}x\mathrm{d}y\\
&\quad \left. + \int_\Omega |u + \varepsilon v - u_0|^2 \mathrm{d}x\mathrm{d}y\right\}\\
&= \int_\Omega \frac{(1-g)\nabla u\cdot\nabla v}{|\nabla u|}\mathrm{d}x\mathrm{d}y + \int_\Omega \frac{g(\nabla u_x\cdot\nabla v_x + \nabla u_y\cdot\nabla v_y)}{|\nabla^2 u|}\mathrm{d}x\mathrm{d}y\\
&\quad + \lambda\int_\Omega (u-u_0)v\mathrm{d}x\mathrm{d}y. \qquad (3.2)
\end{aligned}$$

Recall that Green's formula for the vector field W takes the form

$$\int_\Omega W\cdot\nabla v\,\mathrm{d}x\mathrm{d}y = \int_{\partial\Omega} W\cdot Nv\,\mathrm{d}S - \int_\Omega \nabla\cdot Wv\,\mathrm{d}x\mathrm{d}y. \qquad (3.3)$$

Let $W = \frac{(1-g)\nabla u}{|\nabla u|}$, and let $N = (n_1, n_2)$ denote the unit outer normal vector of $\partial\Omega$. Using (3.3) on the first term of (3.2), we get

$$\begin{aligned}
\int_\Omega \frac{(1-g)\nabla u\cdot\nabla v}{|\nabla u|}\mathrm{d}x\mathrm{d}y &= \int_{\partial\Omega}\frac{(1-g)}{|\nabla u|}\nabla u\cdot Nv\,\mathrm{d}S\\
&\quad - \int_\Omega \nabla\cdot\left(\frac{(1-g)\nabla u}{|\nabla u|}\right)v\mathrm{d}x\mathrm{d}y.
\end{aligned}$$

Let $W_1 = \frac{g\nabla u_x}{|\nabla^2 u|}$ and $W_2 = \frac{g\nabla u_y}{|\nabla^2 u|}$, respectively. Using (3.3) on the second term of (3.2), we get

$$\begin{aligned}
&\int_\Omega \frac{g(\nabla u_x\cdot\nabla v_x + \nabla u_y\cdot\nabla v_y)}{|\nabla^2 u|}\mathrm{d}x\mathrm{d}y\\
&= \int_\Omega \frac{g\nabla u_x}{|\nabla^2 u|}\cdot\nabla v_x\,\mathrm{d}x\mathrm{d}y + \int_\Omega \frac{g\nabla u_y}{|\nabla^2 u|}\cdot\nabla v_y\,\mathrm{d}x\mathrm{d}y\\
&= \int_{\partial\Omega}\left(\frac{g\nabla u_x}{|\nabla^2 u|}\right)\cdot Nv_x + \left(\frac{g\nabla u_y}{|\nabla^2 u|}\right)\cdot Nv_y\,\mathrm{d}S\\
&\quad - \int_\Omega \nabla\cdot\left(\frac{g\nabla u_x}{|\nabla^2 u|}\right)v_x + \nabla\cdot\left(\frac{g\nabla u_y}{|\nabla^2 u|}\right)v_y\mathrm{d}x\mathrm{d}y.
\end{aligned}$$

Now let $W = \left[\nabla\cdot\left(\frac{g\nabla u_x}{|\nabla^2 u|}\right), \nabla\cdot\left(\frac{g\nabla u_y}{|\nabla^2 u|}\right)\right]$. Using (3.3), the second term of the above equality becomes

$$\begin{aligned}
&\int_\Omega \nabla\cdot\left(\frac{g\nabla u_x}{|\nabla^2 u|}\right)v_x + \nabla\cdot\left(\frac{g\nabla u_y}{|\nabla^2 u|}\right)v_y\mathrm{d}x\mathrm{d}y\\
&= \int_\Omega W\cdot\nabla v\,\mathrm{d}x\mathrm{d}y = \int_{\partial\Omega} W\cdot Nv\,\mathrm{d}S - \int_\Omega \nabla\cdot Wv\mathrm{d}x\mathrm{d}y\\
&= \int_{\partial\Omega}\nabla\cdot\left(\frac{g\nabla u_x}{|\nabla^2 u|}\right)n_1 v + \nabla\cdot\left(\frac{g\nabla u_y}{|\nabla^2 u|}\right)n_2 v\,\mathrm{d}S\\
&\quad - \int_\Omega \left(\nabla\cdot\left(\frac{g\nabla u_x}{|\nabla^2 u|}\right)\right)_x v + \left(\nabla\cdot\left(\frac{g\nabla u_y}{|\nabla^2 u|}\right)\right)_y v\mathrm{d}x\mathrm{d}y.
\end{aligned}$$

Therefore we obtain

$$\begin{aligned}
&\frac{\mathrm{d}}{\mathrm{d}\varepsilon}|_{\varepsilon=0} E(u+\varepsilon v)\\
&= \int_{\partial\Omega}\nabla u\cdot Nv\,\mathrm{d}S - \int_\Omega \nabla\cdot\left(\frac{(1-g)\nabla u}{|\nabla u|}\right)v\mathrm{d}S\\
&\quad + \int_{\partial\Omega}\left(\frac{g\nabla u_x}{|\nabla^2 u|}\right)\cdot Nv_x + \left(\frac{g\nabla u_y}{|\nabla^2 u|}\right)\cdot Nv_y\,\mathrm{d}S\\
&\quad - \int_{\partial\Omega}\nabla\cdot\left(\frac{g\nabla u_x}{|\nabla^2 u|}\right)n_1 v + \nabla\cdot\left(\frac{g\nabla u_y}{|\nabla^2 u|}\right)n_2 v\,\mathrm{d}S\\
&\quad + \int_\Omega \left(\nabla\cdot\left(\frac{g\nabla u_x}{|\nabla^2 u|}\right)\right)_x v + \left(\nabla\cdot\left(\frac{g\nabla u_y}{|\nabla^2 u|}\right)\right)_y v\mathrm{d}x\mathrm{d}y\\
&\quad + \lambda\int_\Omega (u-u_0)v\mathrm{d}x\mathrm{d}y.
\end{aligned}$$

With the boundary conditions

$$\begin{aligned}
&\nabla u\cdot N = 0, \quad \nabla u_x\cdot N = 0, \quad \nabla u_y\cdot N = 0,\\
&\nabla\cdot\left(\frac{g\nabla u_x}{|\nabla^2 u|}\right)n_1 = 0, \quad \nabla\cdot\left(\frac{g\nabla u_y}{|\nabla^2 u|}\right)n_2 = 0, \qquad (3.4)
\end{aligned}$$

the associated Euler–Lagrange equation for the energy (3.1) is

$$\begin{aligned}
&-\nabla\cdot\left(\frac{(1-g)\nabla u}{|\nabla u|}\right) + \left(\nabla\cdot\left(\frac{g\nabla u_x}{|\nabla^2 u|}\right)\right)_x + \left(\nabla\cdot\left(\frac{g\nabla u_y}{|\nabla^2 u|}\right)\right)_y\\
&\quad + \lambda(u-u_0) = 0.
\end{aligned}$$

Using the steepest descent method, we thus are able to derive the associated heat flow for our model (3.1),

$$\begin{aligned}
\frac{\partial u}{\partial t} &= \nabla\cdot\left((1-g)\frac{\nabla u}{|\nabla u|}\right) - \left(g\frac{u_{xx}}{|\nabla^2 u|}\right)_{xx} - \left(g\frac{u_{xy}}{|\nabla^2 u|}\right)_{yx}\\
&\quad - \left(g\frac{u_{yx}}{|\nabla^2 u|}\right)_{xy} - \left(g\frac{u_{yy}}{|\nabla^2 u|}\right)_{yy} - \lambda(u-u_0) \quad \text{on} \quad \Omega^T \qquad (3.5)
\end{aligned}$$

with boundary conditions (3.4) on $\partial\Omega^T$ and $u|_{t=0} = u_0$ on Ω, where Ω is an open, bounded Lipschitz domain and $\Omega^T = \Omega\times[0,T]$, $\partial\Omega^T = \partial\Omega\times[0,T]$.

4. Implementation details and experimental results

To discretize the Eq. (3.5), we use the finite difference scheme [6,14,22]. Denote the space step by $h = 1$ and the time step by τ. Thus we have

$$\begin{aligned}
&D_x^{\pm}(u_{i,j}) = \pm[u_{i\pm1,j} - u_{i,j}], \quad D_y^{\pm}(u_{i,j}) = \pm[u_{i,j\pm1} - u_{i,j}],\\
&D_{xx}(u_{i,j}) = D_x^-\left(D_x^+(u_{i,j})\right), \quad D_{xy}^{\pm}(u_{i,j}) = \pm\left[D_y^{\pm}\left(D_x^{\pm}(u_{i,j})\right)\right],\\
&D_{yx}^{\pm}(u_{i,j}) = \pm\left[D_x^{\pm}\left(D_y^{\pm}(u_{i,j})\right)\right], \quad D_{yy}(u_{i,j}) = D_y^-\left(D_y^+(u_{i,j})\right),\\
&|D(u_{i,j})| = \sqrt{\left(D_x^+(u_{i,j})\right)^2 + \left(D_y^+(u_{i,j})\right)^2 + \delta},\\
&|D_x(u_{i,j})| = \sqrt{\left(D_x^+(u_{i,j})\right)^2 + \left(m\left[D_y^+(u_{i,j}), D_y^-(u_{i,j})\right]\right)^2 + \delta},\\
&|D_y(u_{i,j})| = \sqrt{\left(D_y^+(u_{i,j})\right)^2 + \left(m\left[D_x^+(u_{i,j}), D_x^-(u_{i,j})\right]\right)^2 + \delta},\\
&|D^2(u_{i,j})| = \sqrt{\left(D_{xx}(u_{i,j})\right)^2 + \left(D_{xy}^+(u_{i,j})\right)^2 + \left(D_{yx}^+(u_{i,j})\right)^2 + \left(D_{yy}(u_{i,j})\right)^2 + \delta},
\end{aligned}$$

where $m[a,b] = (\frac{\operatorname{sign} a + \operatorname{sign} b}{2}) \cdot \min(|a|,|b|)$ and $\delta > 0$ is near 0.

The details of the numerical algorithm for model (3.1) are given in the following (the subscripts i,j are omitted):

$$u^{k+1} = u^k + \tau\left[D_x^-\left((1-g)\frac{D_x^+u^k}{|D_xu^k|}\right) + D_y^-\left((1-g)\frac{D_y^+u^k}{|D_yu^k|}\right)\right] - \tau\left[D_{xx}\left(g\frac{D_{xx}u^k}{|D^2u^k|}\right) + D_{yx}^-\left(g\frac{D_{xy}^+u^k}{|D^2u^k|}\right) + D_{xy}^+\left(g\frac{D_{yx}^-u^k}{|D^2u^k|}\right) + D_{yy}\left(g\frac{D_{yy}u^k}{|D^2u^k|}\right)\right] - \tau\lambda(u^k - u_0^k). \quad (4.1)$$

The corresponding algorithm for the ROF model and the LLT model is given by setting $g = 0$ and $g = 1$ in (4.1), respectively.

We present the numerical results below. First, we consider a 2-D denoising problem. The results obtained by our model are compared with those of the ROF model as well as the LLT model.

Example 1. The Lena image of size 253×253 is used as a test image. The essential idea of our model is to take the advantage of the ROF model and the LLT model in order to recover both jumps and smooth signals accurately. From Fig. 1, compared with the ROF model and the LLT model, our proposed model yields better results in image restoration since it avoids the staircase effect of the ROF model while at the same time preserving edges as well as the ROF model. In other words, our model is able to combine the advantage of both ROF model and LLT model while doing better than each individually.

The parameters are chosen like this: the larger the noise is, the lager σ is , and the smaller the fidelity coefficient λ is.

In order to evaluate the three models, we show the Signal to Noise Ratio (SNR) of the restored image and the L^2-norm of the difference between the restored and the original image. For a given true image u and its noisy observation u_0, the noise is denoted as $n = u_0 - u$. With this, the formulas used to calculate the SNR and the L^2-norm become

$$\mathrm{SNR} = 20 \cdot \log_{10}\left(\frac{\int_\Omega (u_0 - \bar{u}_0)^2 \mathrm{d}x\,\mathrm{d}y}{\int_\Omega (n - \bar{n})^2 \mathrm{d}x\,\mathrm{d}y}\right),$$

$$L^2\text{-norm} = \int_\Omega (u_0 - u)^2 \mathrm{d}x\,\mathrm{d}y,$$

Table 1
SNR, L^2-norm and $\tau_{\max}$ for the different models

Model	SNR	L^2-norm	$\tau_{\max}$(CFL)
ROF	13.70	$2.82 \cdot 10^5$	1.25
LLT	14.61	$1.85 \cdot 10^5$	0.21
Our proposed model	16.08	$1.69 \cdot 10^5$	0.43

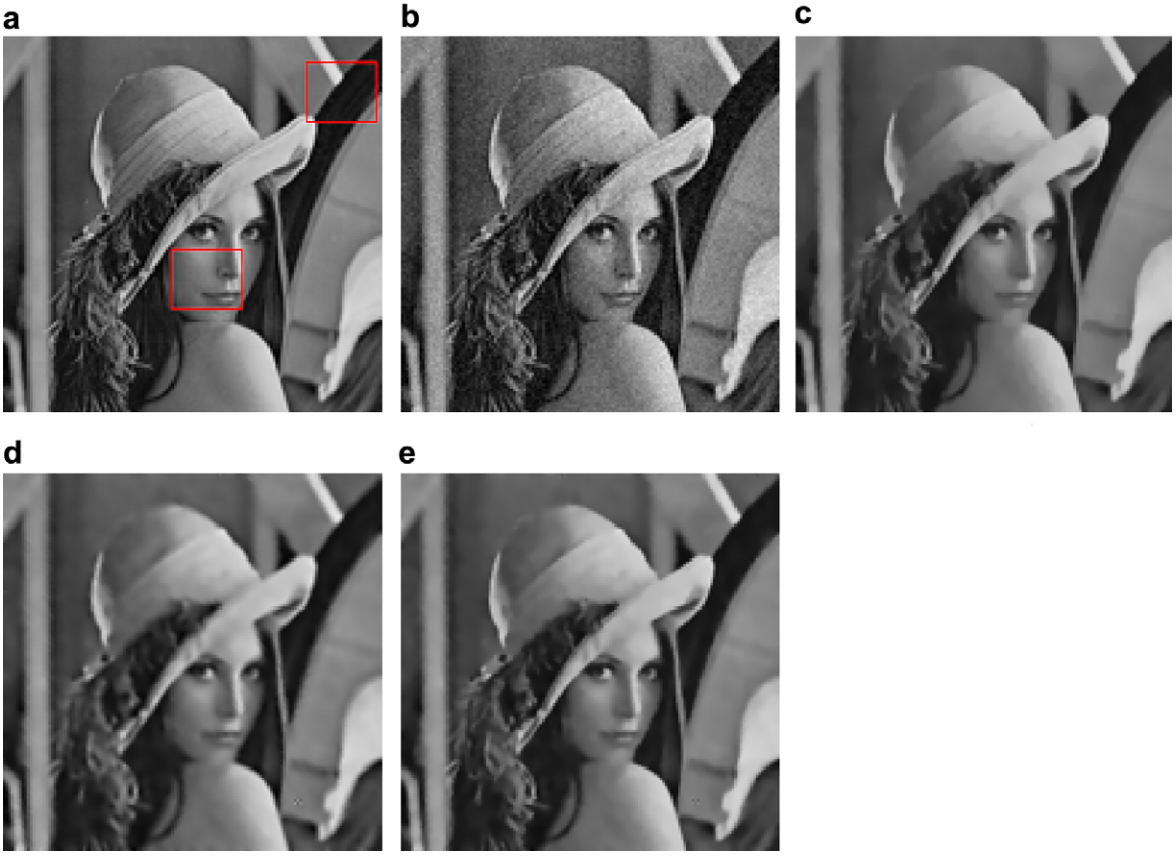

Fig. 1. 2-D denoising. (a) The original Lena image. The red rectangles indicate two regions of special interest which will be zoomed-in Figs. 2 and 3; (b) Lena image corrupted with Gaussian noise with SNR = 10.34 db; (c) restoration by the ROF model (iteration = 60, $\tau = 0.3$); (d) restoration by the LLT model (iteration = 300, $\tau = 0.05$); (e) restoration by our proposed model (iteration = 300, $\tau = 0.05$). (other parameters: $k = 0.005$, $\lambda = 0.01$, $\sigma = 0.5$, $\delta = 0.001$, $\gamma = 0.0001$). (For interpretation of the references to colour in this figure legend, the reader is referred to the web version of this article.)

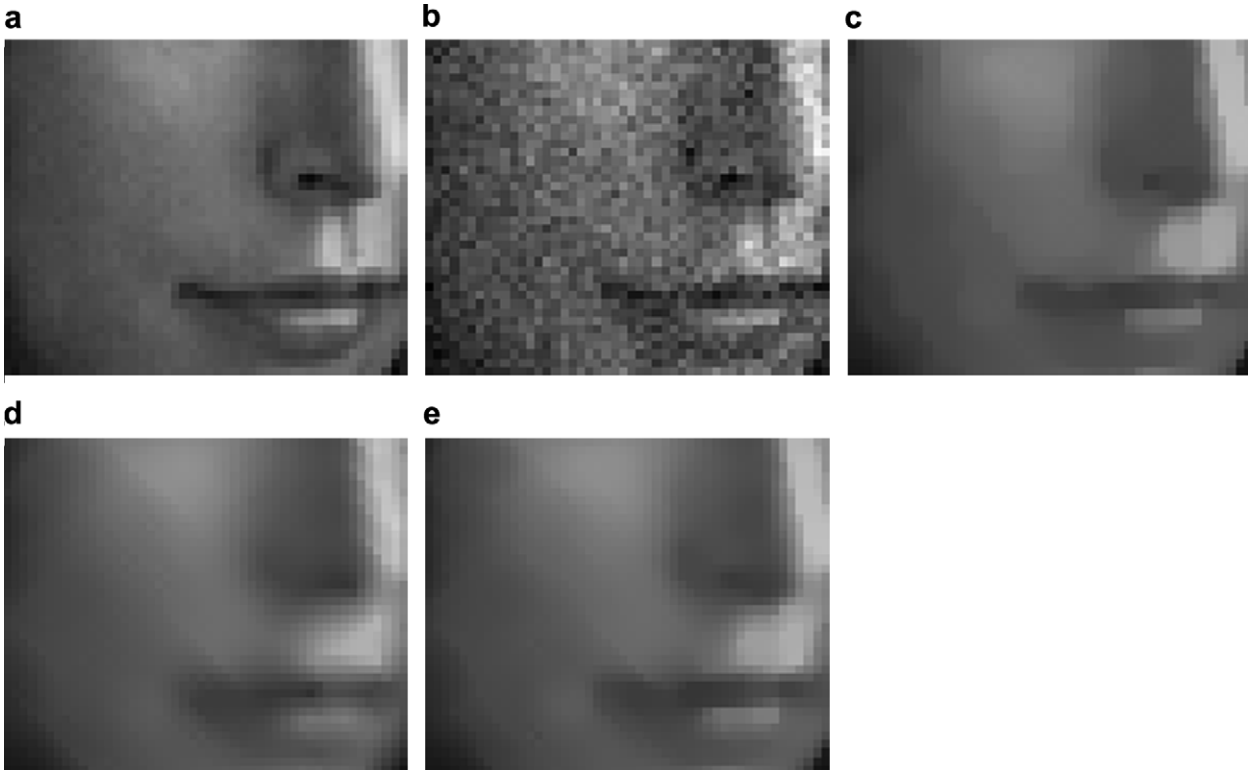

Fig. 2. A small part of Lena image is emphasized to compare the performance of the three models when processing with smooth regions. (a) True image; (b) noisy image; (c) restoration by the ROF model; (d) restoration by the LLT model; (e) restoration by our proposed model.

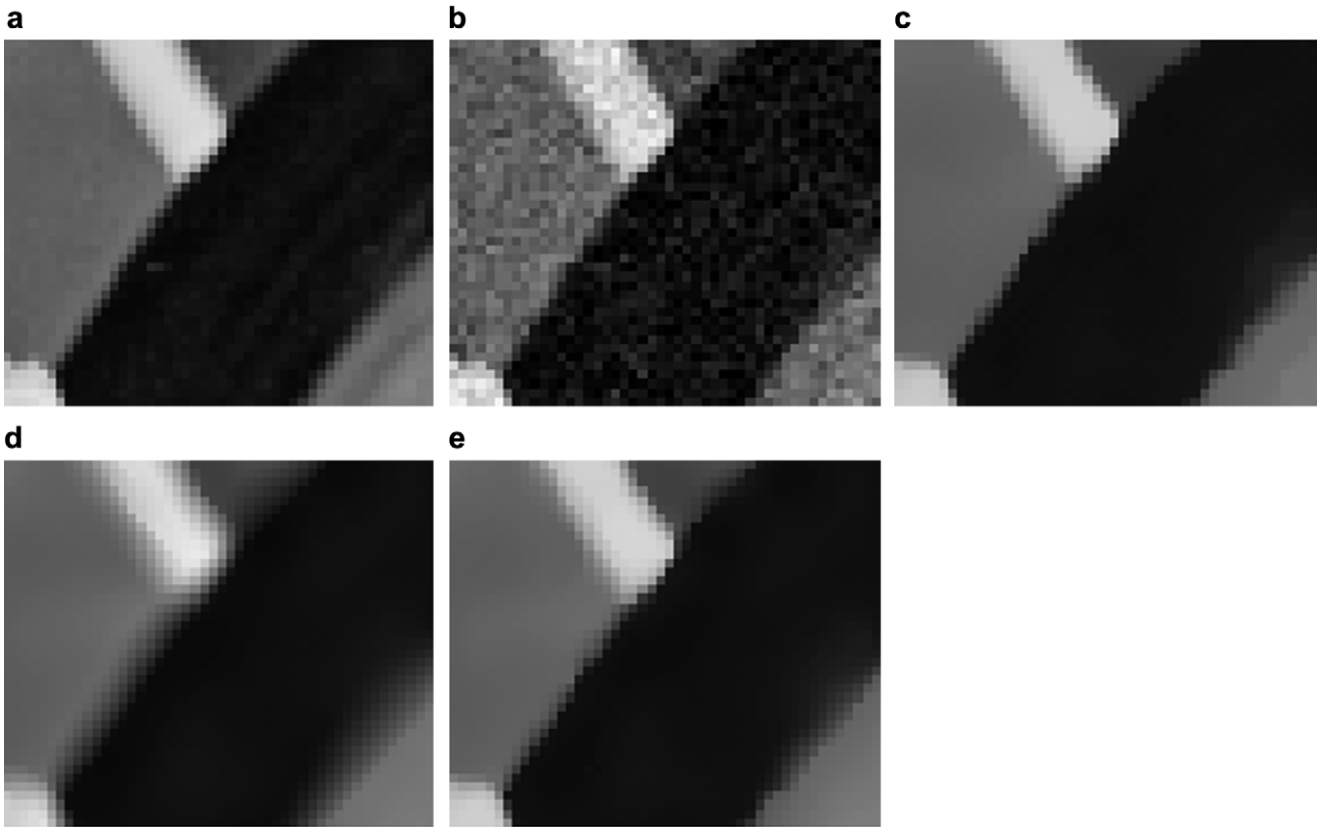

Fig. 3. A small portion of Lena image is emphasized to show the difference of the three models when processing regions with discontinuities. (a) True image; (b) noisy image; (c) restoration by the ROF model; (d) restoration by the LLT model; (e) restoration by our proposed model.

where

$$\bar{u}_0 = \frac{1}{|\Omega|}\int_\Omega u_0 \mathrm{d}x\,\mathrm{d}y, \quad \bar{n} = \frac{1}{|\Omega|}\int_\Omega n \mathrm{d}x\,\mathrm{d}y.$$

Before processing, the noisy Lena image has SNR = 10.34 db and L^2-norm $= 3.82 \cdot 10^5$. For each scheme, we found a maximum time step $\tau_{\max}$ where, when $\tau > \tau_{\max}$, the iterative scheme is unstable and the iterative solution

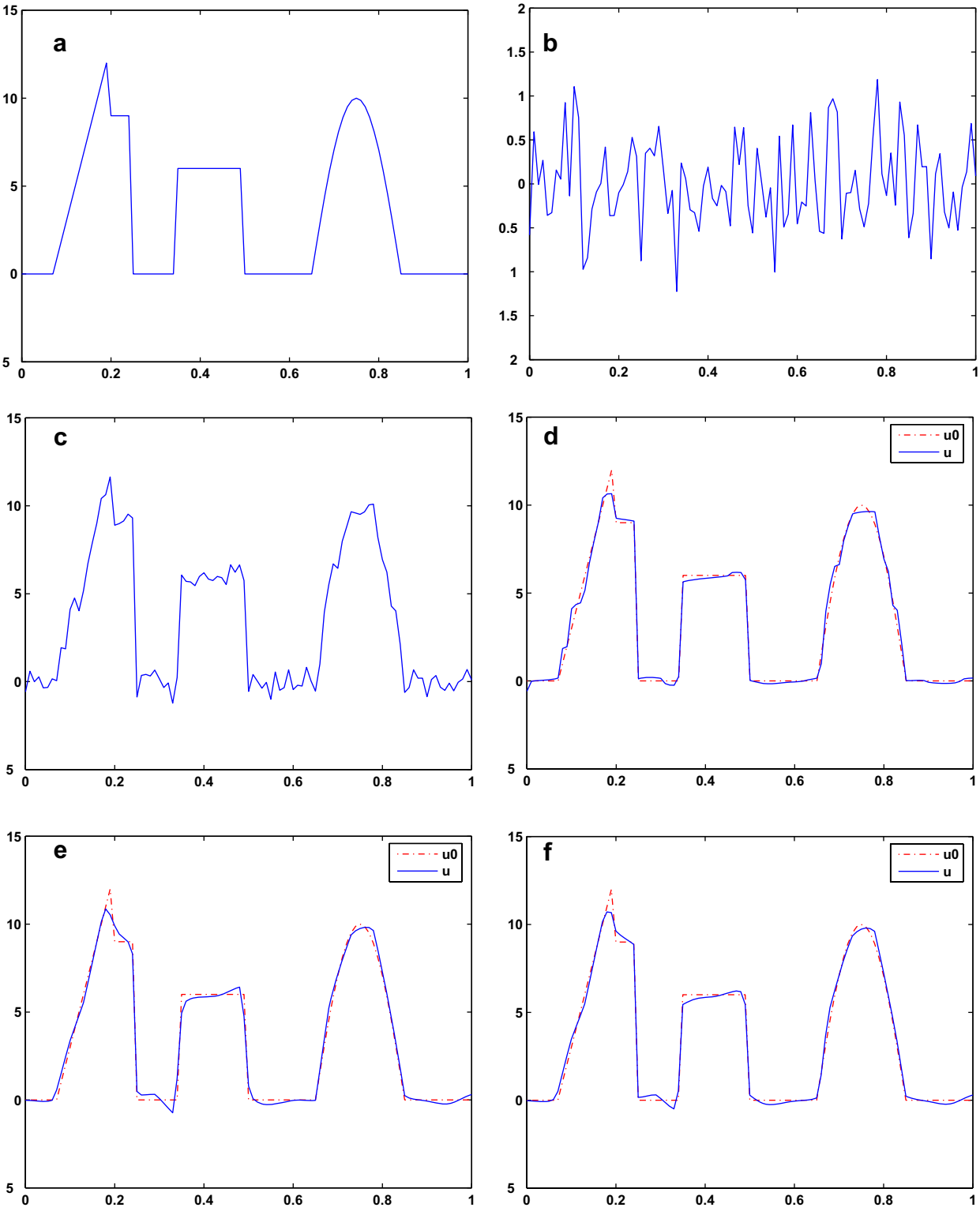

Fig. 4. 1-D denoising. (a) Initial clean signal; (b) noisy signal, SNR = 35.30 db, L^2-norm = 24.93; (c) Gaussian noise with standard deviation 0.5, and mean 0; (d) recovered from ROF model, SNR = 41.52 db, L^2-norm = 12.00; (e) recovered from LLT model, SNR = 39.76 db, L^2-norm = 14.67; (f) recovered from our proposed model, SNR = 44.02 db, L^2-norm = 9.00; (iteration = 100, other parameters: $k = 0.5$, $\tau = 0.005$, $\lambda = 0.01$, $\sigma = 0.5$, $\delta = 0.001$, $\gamma = 0.0001$).

explodes. On the other hand, when $\tau \leqslant \tau_{\max}$, the solutions converge to a steady state. $\tau_{\max}$ is determined through numerous experiments on Lena image as in [14].

From Table 1, we observe that our proposed model has a higher SNR than either the ROF model or the LLT model, and at the same time, the L^2-norm is the smallest among the three models. Therefore, we conclude that the proposed model does the best job among the three models. Moreover, we observe that the maximum time step of the proposed model is larger than that of the LLT model.

In order to better understand the behavior of the proposed model in local regions, especially in regions with smooth signals and regions with discontinuities, we present the following zoomed-in local results.

A small part of the Lena image is shown in Fig. 2. It is clear that the ROF model transforms smooth regions into piecewise constant regions. Our proposed model and the LLT model both process smooth regions better than the ROF model. However, the LLT model may cause blurring in the face while our model is clearer.

Next, we evaluate the performance of the three different methods in regions with edges. In Fig. 3, our proposed model, as well as the ROF model, restores and enhances such signals better than the LLT model.

With our model is established for 2-D images, we can turn to the 1-D case. Note that the related numerical scheme should be changed as follows:

$$D_x^{\pm}(u_i) = \pm[u_{i\pm1} - u_i], \quad D_{xx}(u_i) = D_x^{-}\left(D_x^{+}(u_i)\right),$$
$$|D(u_i)| = \sqrt{\left(D_x^{+}(u_i)\right)^2 + \delta}, \quad |D^2(u_i)| = \sqrt{\left(D_{xx}(u_i)\right)^2 + \delta},$$

where $\delta > 0$ is a parameter. The details of the numerical algorithm for model (3.1) in 1-D are given by (the subscript i is omitted):

$$u^{k+1} = u^k + \tau\left(D_x^{-}\left((1-g)\frac{D_x^{+}u^k}{|Du^k|}\right) - D_{xx}\left(g\frac{D_{xx}u^k}{|D^2u^k|}\right) - \lambda\left(u^k - u_0^k\right)\right). \tag{4.2}$$

The corresponding algorithms for the ROF model and the LLT model are obtained by setting $g = 0$ and $g = 1$ in (4.2), respectively.

Now, we apply our algorithm to a signal with size 50 containing 'ramps' and 'parabolas'.

Example 2. Fig. 4 shows the clean signal u and the noisy signal $u_0 = u + n$, where n is Gaussian noise with standard deviation, STD = 0.5 and mean = 0. The figure also shows the restoration results with the ROF model, the LLT model and our proposed model. Visually, our proposed model has less staircase effects and makes a good compromise between edge preserving and smoothing. We also give estimates of SNR and L^2-norm to show that our proposed model is the best among the three models.

All these experimental results show that our model is effective in image restoration and works as expected theoretically.

5. Conclusion

This paper describes a method for filtering gray scale images corrupted by Gaussian noise. The proposed method combines a second-order filter (the ROF filter) and a fourth-order PDE filter (the LLT filter). The model is based on a convex combination of the two models and the combining function is controlled by the observed image. We have tested our algorithm on images consisting of edges and smooth regions. From these experimental results, we observed that the proposed method is able to preserve edges as well as the ROF model while at the same time avoiding the staircase effects in smooth regions. In a word, the combined model reaps benefits of both the ROF model and the LLT model, surpassing each individually in image restoration. Comparing with the iterative method in [22], our model is more natural. Furthermore, some theoretical results are presented. In the future, we plan to study the evolution Eq. (3.5) and the associated heat flow for energy (2.1) theoretically.

Acknowledgment

This work is supported by the National Science Foundation of China (No. 10671066) and the National Basic Research Program (973 Program, No. 2006CB708305).

References

[1] L.C. Evans, R.F. Gariepy, Measure Theory and Fine Properties of Functions, CRC Press, Boca Raton, FL, 1992.
[2] F. Giusti, Minimal Surfaces and Functions of Bounded VariationMonographs in Math., vol. 80, Birkhäuser, Basel, 1984.
[3] R. Acar, C.R. Vogel, Analysis of bounded variation penalty methods for ill-posed problems, Inverse Probl. 10 (1994) 1217–1229.
[4] A. Chambolle, P.L. Lions, Image recovery via total variation minimization and related problems, Numer. Math. 76 (1997) 167–188.
[5] M. Lysaker, S. Osher, X.C. Tai, Noise removal using smoothed normals and surface fitting, IEEE Trans. Image Process. 13 (10) (2004) 1345–1357.
[6] L. Rudin, S. Osher, E. Fatemi, Nonlinear total variation based noise removal algorithms, Physica D 60 (1992) 259–268.
[7] Y.M. Chen, M. Rao, Minimization problems and associated flows related to weighted p energy and total variation, SIAM J. Math. Anal. 34 (2003) 1084–1104.
[8] Y.M. Chen, T. Wunderli, Adaptive total variation for image restoration in BV space, J. Math. Anal. Appl. 272 (2002) 117–137.
[9] P. Blomgren, T.F. Chan, P. Mulet, C. Wong, Total variation image restoration: Numerical methods and extensions, in: Proceedings, IEEE International Conference on Image Processing, III, 1997, pp. 384–387.
[10] M. Nikolova, Weakly constrained minimization: application to the estimation of images and signals involving constant regions, J. Math. Imaging Vis. 21 (2004) 155–175.
[11] A. Chambolle, P.L. Lions, Image recovery via total variation minimization and related problems, Numer. Math. 76 (1997) 167–188.
[12] T. Chan, A. Marquina, P. Mulet, High-order total variation-based image restoration, SIAM J. Sci. Comput. 22 (2000) 503–516.
[13] Y.L. You, M. Kaveh, Fourth-order partial differential equation for noise removal, IEEE Trans. Image Process. 9 (10) (2000) 1723–1730.
[14] M. Lysaker, A. Lundervold, X.C. Tai, Noise removal using fourth-order partial differential equation with applications to medical

magnetic resonance images in space and time, IEEE Trans. Image Process. 12 (12) (2003) 1579–1590.
[15] S. Osher, A. Sole, L. Vese, Image decomposition and restoration using total variation minimization and the H^1 norm, Multiscale Model. Simul. 1 (3) (2003) 349–370.
[16] S. Osher, O. Scherzer, G-norm properties of bounded variation regularization, Comm. Math. Sci. 2 (2) (2004) 237–254.
[17] A. Obereder, S. Osher, O. Scherzer, On the use of dual norms in bounded variation type regularization, UCLA cam report 04–35. Available from: <http://www.math.ucla.edu/applied/cam/>.
[18] S. Didas, B. Burgeth, A. Imiya, J. Weickert, Regularity and scale-space properties of fractional high order linear filtering, in: R. Kimmel, N. Sochen, J. Weickert (Eds.), Scale-space and PDE Methods in Computer Vision. Lecture Notes in Computer Science, vol. 3459, Springer, Berlin, 2005.
[19] S. Didas, J. Weickert, B. Burgeth, Stability and local feature enhancement of higher order nonlinear diffusion filtering, in: W. Kropatsch, R. Sablatnig, A. Hanbury (Eds.), Pattern Recognition. Lecture Notes in Computer Science, vol. 3663, Springer, Berlin, 2005, pp. 451–458.
[20] J.B. Greer, A.L. Bertozzi, H^1 solutions of a class of fourth order nonlinear equations for image processing, in: V. Chepyzhov, M. Efendiev, A. Miranville, R. Temam (Eds.), Discrete and Continuous Dynamical Systems 2004, special issue in honor of Mark Vishik, vol. 1–2, No. 10, 2004, pp. 349–366.
[21] J.B. Greer, A.L. Bertozzi, Traveling wave solutions of fourth order PDEs for image processing, SIAM. J. Math. Anal. 36 (1) (2004) 38–68.
[22] M. Lysaker, X.C. Tai, Iterative image restoration combining total variation minimization and a second-order functional, Int. J. Comput. Vision 66 (1) (2006) 5–18.